

The *Drosophila* Formin Fhod Nucleates Actin Filaments

Aanand A. Patel¹, Zeynep A. Oztug Durer^{2,*}, Aaron P. van Loon¹, and Margot E. Quinlan^{2,3,#}

¹Molecular Biology Interdepartmental Doctoral Program, University of California Los Angeles, Los Angeles, California 90095

²Department of Chemistry and Biochemistry, University of California Los Angeles, Los Angeles, California 90095

³Molecular Biology Institute, University of California Los Angeles, Los Angeles, California 90095

*Current address: Department of Biophysics, Acibadem University School of Medicine, Istanbul, Turkey

Running title: *Fhod nucleates actin*

[#]To whom correspondence should be addressed: Prof. Margot E. Quinlan, Department of Chemistry and Biochemistry, 611 Charles E. Young Dr. E., University of California, Los Angeles, CA 90095. Tel.: 310-206-8064; Fax: 310-206-5213; E-mail: Margot@chem.ucla.edu.

Keywords: actin, cytoskeleton, *Drosophila*, formin, Fhod, Fhos, processivity, TIRF

ABSTRACT

Formins are a conserved group of proteins that nucleate and processively elongate actin filaments. Among them, the formin homology domain-containing protein (FHOD) family of formins contributes to contractility of striated muscle and cell motility in several contexts. However, the mechanisms by which they carry out these functions remain poorly understood. Unlike other formins, mammalian FHOD1 and FHOD3 do not accelerate actin assembly *in vitro*, and have instead been suggested to act as barbed end cappers or bundlers. Here, we show that purified *Drosophila* Fhod, in contrast with the mammalian homologues, potently accelerates actin assembly by nucleation. We found that Fhod binds tightly to barbed ends, where it slows elongation in the absence of profilin and allows elongation in the presence of profilin. Fhod protects barbed ends from capping protein, but dissociates from barbed ends relatively quickly. Finally, we used cosedimentation assays to determine that Fhod binds the sides of actin filaments and bundles filaments. This work establishes that Fhod shares the capacity of other formins to nucleate and bundle actin filaments, but is notably less effective at processively elongating barbed ends.

Formins are a major, conserved group of proteins known for their ability to both nucleate new actin filaments and remain processively associated with fast-growing barbed ends via their formin homology 2 (FH2) domains. While bound to the barbed end, many formins accelerate elongation through their proline-rich FH1 domains, which recruit profilin-bound actin monomers to the barbed end. In addition to these classic activities, some formins have additional effects on actin filaments, such as severing, bundling, or cross-linking to microtubules (1). Animals have seven formin families, which share the same domain structure, including the highly conserved FH2 domains. Importantly, formins differ in their actin assembly activities and modes of regulation, allowing them to fulfill distinct cellular roles.

The formin homology domain-containing (FHOD) family of formins has two mammalian isoforms, FHOD1 and FHOD3, which assemble contractile actin structures in several contexts. FHOD1 is widely expressed and assembles stress fibers that contribute to the adhesion, spreading, and motility of numerous cell types (2–8). FHOD3 has also been implicated in the motility of some cancers (9, 10), but its expression is predominantly restricted to striated muscle (11, 12). In

cardiomyocytes, FHOD3 localizes to the sarcomere and is required for its assembly and maintenance (12–15). Finally, changes in expression level and polymorphisms of both FHOD1 and FHOD3 are associated with cardiomyopathies (12, 16–19).

The mechanisms by which FHOD family members function remain poorly understood. Unlike other formins, purified FHOD1 and FHOD3 were shown to slow, rather than accelerate, actin assembly *in vitro*, and have therefore been suggested to act as actin cappers or bundlers (13, 20). In contrast, the cell biology data suggest that FHOD1 and FHOD3 function as actin nucleators *in vivo*. Across a wide range of cell types, expression of constitutively active FHOD1 or FHOD3 is sufficient to induce the formation of stress fibers (2–5, 13). Furthermore, FHOD3 is required for sarcomere assembly following latrunculin washout (12). These data are most suggestive of actin nucleation, although FHOD1 and FHOD3 might instead function by stabilizing or reorganizing existing actin filaments.

Drosophila melanogaster has a single FHOD family member, referred to here as Fhod (also known as Fhos or knittig). The Fhod gene is alternatively spliced to produce eight different isoforms, which maintain constant FH1 and FH2 domains but alter their regulatory N-termini and C-terminal tails. The role of FHOD proteins in cell motility and contractility is well conserved in *Drosophila*, as Fhod contributes to motility in macrophages and tracheal tip cells (21), sarcomere organization in striated muscle (22, 23), and cardiac contractility (16). Here, we show that purified *Drosophila* Fhod, unlike its mammalian homologues, potentially accelerates actin assembly by nucleation. Fhod remains processively associated with the barbed end, where it slows elongation in the absence of profilin and allows elongation, at rates similar to actin alone, in the presence of profilin. Although Fhod does not accelerate barbed end elongation, we find that Fhod protects barbed ends from capping protein with a characteristic run length of about 2 μ m. Fhod additionally binds tightly to the sides of filaments and bundles filaments together.

RESULTS

Fhod accelerates actin assembly—We purified the C-terminal half of *Drosophila* Fhod

isoform A, encompassing the FH1 domain, FH2 domain, and C-terminal tail (Fig 1A). This isoform is sufficient to rescue viability in Fhod null flies (21), and its C-terminus is identical to that of isoform H, which rescues sarcomere organization in indirect flight muscle (22). We first tested the effect of Fhod on the assembly of *Acanthamoeba* actin in bulk pyrene assays; Fhod potentially accelerated actin assembly in a dose-dependent manner (Fig 1B–C). In previous work, purified FHOD1 and FHOD3 did not accelerate assembly of actin from rabbit skeletal muscle (13, 20). Because the activity of some formins depends on the actin isoform (W. T. Silkworth et. al., manuscript submitted), we also tested the ability of Fhod to assemble rabbit muscle actin. We observed similarly accelerated actin assembly with muscle actin and *Acanthamoeba* actin (data not shown). Because Fhod is expressed in both muscle and non-muscle cells, it is logical that Fhod would function equally well with muscle and non-muscle actin. All subsequent experiments were performed with *Acanthamoeba* actin.

To further compare Fhod to characterized formins, we introduced two classical mutations, I966A and K1112A, in conserved residues of the FH2 domain (24). The I966A mutation almost completely abolished activity, whereas the K1112A mutation markedly reduced, but did not eliminate, activity (Fig 1D). We also tested the ability of Fhod to promote actin assembly in the presence of profilin, which binds most actin monomers in the cell and inhibits spontaneous nucleation. Profilin strongly impaired actin assembly by Fhod, but Fhod still accelerated actin assembly in a dose-dependent manner under these conditions (Fig 1E). Fhod is thus similar to other studied formins.

Fhod promotes actin nucleation but not elongation—Because formins are capable of promoting nucleation as well as elongation, we investigated the relative contributions of these activities. We assessed nucleation activity by imaging actin filaments polymerized in the absence or presence of Fhod. Fhod greatly increased the number of filaments per field of view, indicating that Fhod promotes actin assembly by nucleation (Fig 2A–B).

We then asked how Fhod affects barbed end elongation. Formins typically slow elongation in the absence of profilin and accelerate elongation

in the presence of profilin. Using bulk seeded elongation assays, we found that Fhod slows barbed end elongation in the absence of profilin with an affinity of 19 nM (Fig 2C, E). In the presence of profilin, Fhod had a minimal effect on elongation at most concentrations we tested (Fig 2D). At high concentrations of Fhod, the elongation rate appeared to decrease; we attribute this decrease to filament bundling (see below) rather than a true effect on barbed end elongation because the trend does not follow the same dose-dependence we observed in the absence of profilin, and high concentrations of Fhod also caused substantial fluorescence artifacts in actin depolymerization assays. To confirm that Fhod does not alter barbed end elongation in the presence of profilin, we directly measured elongation rates using total internal reflection fluorescence (TIRF) microscopy. In agreement with our bulk assays, we detected no difference in elongation rates (Fig 2F-G).

Because we did not observe clear evidence of processive elongation by Fhod, we used several additional assays to verify and characterize the interaction between Fhod and barbed ends. We first verified barbed end binding in bulk barbed end depolymerization assays. The dose dependence gives us an additional measure of the affinity between Fhod and barbed ends. Fhod inhibited actin depolymerization with a K_d of 5 nM, similar to our measurement from the seeded elongation assays (Fig 3A-B). We then used actin reannealing assays, in which two colors of sheared actin filaments were mixed and allowed to reanneal. Fhod inhibited actin reannealing, indicating that it binds barbed ends and can remain bound on the timescale of minutes (Fig 3C). Thus Fhod binds barbed ends tightly, like other formins, but does not accelerate elongation, unlike other formins.

Fhod antagonizes capping protein—We measured the ability of Fhod to antagonize capping protein, which binds tightly to barbed ends and prevents elongation. In bulk seeded elongation assays, 6 nM capping protein was sufficient to completely abolish actin elongation. Fhod abrogated this effect when added to F-actin seeds prior to capping protein (Fig 4A). We fit these data to a competition binding equation to determine that Fhod has an apparent K_d of 7 nM for growing barbed ends (Fig 4B), consistent with

our previous measurements. Recent evidence suggests that formins can antagonize capping protein not only by passive competition for the barbed end, but also by binding capped barbed ends and actively displacing capping protein (25, 26). However, filaments did not grow when capping protein was added before Fhod (data not shown), indicating that the actin elongation we observed was due to Fhod processively protecting the barbed end, and not due to Fhod actively displacing capping protein from barbed ends.

We used TIRF microscopy to observe competition between Fhod and capping protein on individual filaments. We incubated seeds with Fhod prior to adding capping protein and actin monomers, then measured how long Fhod could protect the growing barbed end. Consistent with our bulk assays, we found that barbed ends were completely capped by capping protein in the absence of Fhod, but were able to grow in the presence of Fhod. Because the vast majority of filaments were capped by the time we could start imaging (2-3 minutes after the start of polymerization), we measured filament lengths in static images taken 5 minutes after addition of actin monomers (Fig 4C-D). By fitting the filament lengths to a single exponential curve, we determined that Fhod has a characteristic run length of 2 μ m (Fig 4E). This provides us with an approximate measure of Fhod's processivity, with two assumptions: (1) capping protein binds to barbed ends as soon as Fhod dissociates, and (2) capping protein does not cap barbed ends that are already bound by Fhod. The first assumption is consistent with the strong affinity (~ 0.4 nM) of capping protein for barbed ends. However, the ability of capping protein to bind mDia1-bound barbed ends and displace mDia1 (25, 26) suggests that capping protein might also bind Fhod-bound barbed ends, which would make our measurement of Fhod's processivity an underestimate.

Fhod bundles actin filaments—Finally, we asked whether Fhod shares the capacity of other formins to bind the sides of actin filaments and bundle them. In high speed cosedimentation experiments, Fhod pelleted with F-actin, demonstrating that Fhod binds the sides of actin filaments, with a K_d of 180 nM (Fig 5A). In low-speed cosedimentation, Fhod increased the amount of F-actin in the pellet, indicating that it forms actin bundles (Fig 5B). We used TIRF microscopy

to determine the polarity of actin bundles formed by Fhod. Actin bundles typically elongated from both ends, indicating that the actin filaments in these bundles were not arranged exclusively in parallel (Fig 5C).

DISCUSSION

Here, we show that *Drosophila* Fhod shares the classic activities of formins, actin nucleation and processive elongation, with the additional capacity to bundle actin filaments. These observations differ substantially from those reported for mammalian FHOD1 and FHOD3. Whereas both FHOD1 and FHOD3 were reported to slow actin assembly (13, 20), we found that *Drosophila* Fhod is a potent actin nucleator similar to other formins. Our ability to achieve high expression in *E. coli*, in contrast with the requirement of a eukaryotic expression system for human FHOD1 (20), indicates a difference in the folding, conformation, or stability of the two proteins. Therefore, we expect that FHOD1 and FHOD3 might function as actin nucleators *in vivo*, despite their inability to accelerate actin assembly *in vitro*. FHOD1 and FHOD3 induce the formation of stress fibers in several cell types (2–5, 13), and FHOD3 is required for sarcomere assembly (12). These functions are well conserved in *Drosophila* (21, 22) and most consistent with actin nucleation. However, it remains formally possible that FHOD proteins instead stabilize or bundle filaments that are polymerized by a different actin nucleator. Future work will be needed to determine what accounts for the differences we observe between *Drosophila* and mammalian FHOD proteins.

We did not observe evidence of accelerated barbed end elongation with Fhod. This is not unprecedented, as some formins such as *Drosophila* Daam (27) and mouse FMNL1 (28) either slow barbed end elongation or leave the elongation rate unchanged in the presence of profilin. Mammalian FHOD1 and FHOD3 were also shown to slow barbed end elongation, but in a profilin-independent manner (13, 20). We expect that both the FH1 and FH2 domains contribute to Fhod's inability to accelerate barbed end elongation. The slow barbed end elongation in the absence of profilin is suggestive of an FH2 domain that spends most of the time in a closed conformation, similar to Cdc12 (29). The addition of profilin restores the elongation rate to that of

actin alone, indicating that the FH1 domain has some ability to recruit profilin-actin, but perhaps not as effectively as the FH1 domains of other formins. The effectiveness of polyproline tracks in the FH1 domain depend on the number of prolines and their distance from the FH2 domain (30, 31). The polyproline tracks of the Fhod FH1 domain are located relatively far from the FH2 domain, with the closest track (PPPMMP) located 31 residues from the FH2 domain. For comparison, the weak elongator Cdc12 has its closest polyproline track 26 residues away from the FH2 domain, whereas the strong elongators Bni1 and mDia1 have their closest polyproline tracks 22 and 16 residues away, respectively.

We approximate that Fhod has a characteristic run length of 2 μm , which is equivalent to a dissociation rate of $\sim 0.01 \text{ s}^{-1}$ based on the elongation rate of 8 subunits/second. This dissociation rate is an order of magnitude faster than mDia1 and several orders of magnitude faster than mDia2, Bni1, Cdc12, and Capu (32, 33), which does not fit the general trend of faster elongation rates resulting in faster dissociation rates (30). We observed evidence of Fhod protecting barbed ends only when Fhod was incubated with seeds and actin monomers in a tube prior to introducing the mixture onto the surface. This suggests that the surface hinders Fhod's processivity, making our measurement of Fhod's processive elongation activity an underestimate. However, that Fhod is sensitive to conditions that do not perturb the processivity of other formins may indicate that processive elongation is not a critical activity of Fhod. FHOD family members generally localize to the relatively short actin filaments found in stress fibers and the sarcomere, which likely do not require accelerated barbed end growth. Therefore, Fhod's nucleation and bundling activities might be more important in these contexts. We found that Fhod is indeed a potent actin bundler; its affinity of 0.18 μM for sides of actin filaments is comparable to the formins Fus1 (34) and AFH1 (35), and an order of magnitude stronger than mDia1 (36), Daam (27), and Capu (33). Alternatively, it is possible that Fhod accelerates actin elongation *in vivo* through collaborations with other proteins; for example, CLIP-170 was recently shown to augment the processive elongation of mDia1 (37).

EXPERIMENTAL PROCEDURES

Protein expression, purification, and labeling—cDNA for *Drosophila* Fhod isoform A (SD08909, obtained from FlyBase) was used as a template to clone the C-terminal half of Fhod (residues 638-1393) into a modified version of the pET15b plasmid with an N-terminal 6xHis tag. Point mutations were generated by site-directed mutagenesis as described (38). Fhod constructs were transformed in Rosetta(DE3) cells (Novagen), which were grown in 1 liter of Terrific Broth supplemented with 100 mg/L ampicillin and 32 mg/L chloramphenicol. When the OD reached ~0.8, expression was induced by adding 0.25 mM IPTG and shaking overnight at 18 °C. Cells were harvested by centrifugation, washed in PBS, and flash frozen in liquid nitrogen.

Cell pellets were thawed in extraction buffer (10 mM MOPS pH 7, 0.5% Triton X-100, 1 mM DTT, 1 mM PMSF, 2 µg/mL DNaseI). All subsequent steps were performed on ice or at 4 °C. Cells were lysed by microfluidizing, cleared by centrifugation at 20,000 x *g* for 20 minutes, then purified using a HitrapSP-FF cation exchange column (GE Life Sciences) with a gradient of 0.3-1 M NaCl over 16 column volumes. Pooled fractions were diluted at least six-fold into 10 mM Tris pH 8, 1 mM DTT and further purified on a MonoQ anion exchange column (GE Life Sciences) with a gradient of 40-500 mM NaCl over 50 column volumes. Peak fractions were exchanged into storage buffer (10 mM Tris pH 8, 150 mM NaCl, 1 mM DTT, 0-20% glycerol), centrifuged at 20,000 x *g* for 20 minutes, flash frozen in liquid nitrogen, and stored at -80 °C. Fhod protein concentrations were determined using the absorbance at 280 nm with an extinction coefficient of 122,840 M⁻¹ cm⁻¹ (ProtParam), which was verified by comparing the absorbances of native and denatured protein. All Fhod concentrations are reported in terms of dimer concentrations.

Acanthamoeba castellanii actin was purified (39) and labeled with Alexa Fluor 594 succinimidyl ester (40), pyrene iodoacetamide (39), or EZ-link maleimide-PEG2-biotin (Thermo Scientific) (41) according to published protocols. *S. pombe* profilin was purified as described (28) on a polyproline column kindly provided by the Reisler lab (University of California, Los Angeles). The concentration was determined using

the absorbance at 280 nm with an extinction coefficient of 1.63 OD/mg/mL (42). Mouse capping protein was purified as described (43).

Pyrene assays—Pyrene assays were performed essentially as described (44) on an Infinite 200 Pro plate reader (Tecan). In all assays, Fhod was diluted in storage buffer before addition to polymerization buffer to improve stability. The concentration of barbed ends was calculated from the slope (obtained by linear regression over 90 seconds) using the equation [be] = elongation rate/(*k*₊[G-actin] - *k*₋), where *k*₊ = 11.6 µM⁻¹ s⁻¹ and *k*₋ = 1.4 s⁻¹ (45). For seeded elongation assays, actin filaments were sheared by passing three times through a 24-gauge needle, then aliquoted into each well of a clear microplate. Proteins were added to the seeds and incubated for 2-4 minutes at room temperature; in experiments with both Fhod and capping protein, capping protein was added 2-4 minutes after addition of Fhod. Seeds and additional proteins in KMEH (10 mM HEPES pH 7, 1 mM EGTA, 50 mM KCl, 1 mM MgCl₂) were added to Mg-actin to initiate actin elongation. Elongation rates were determined by linear regression over the first 90 seconds and normalized against the rate of actin alone in each experiment. For experiments without capping protein, the affinity of Fhod for barbed ends was determined by fitting the data to the simplified binding equation, *r* = [Fhod] / ([Fhod] + *K*_d) * *a* + *b*, where *r* is the normalized elongation rate. Data for capping protein experiments were analyzed using a competition binding model (46). The following equation was used to determine the *K*_d of Fhod for growing barbed ends:

$$r = \left(1 - \frac{1}{K_{d1} \frac{[Fhod] + K_{d2}}{K_{d2}R_0} + 1} \frac{[CP]}{[be]} \right) * a + b$$

where *r* is the normalized elongation rate, *K*_{d1} is the affinity of capping protein for barbed ends (0.4 nM, measured in a seeded elongation assay in the absence of Fhod), *K*_{d2} is the affinity of Fhod for barbed ends, and *R*₀ is the concentration of free barbed ends when [Fhod]=0. The total concentration of barbed ends was calculated from the initial slope of the polymerization trace for actin alone as described above.

For depolymerization assays, 1 µM F-actin (70% pyrene-labeled) was incubated for at least 15 minutes at room temperature, then

depolymerized by diluting 10-fold in 1x KMEH with additional proteins. The depolymerization rate was determined by linear regression over the first 90 seconds. The affinity of Fhod for barbed ends was determined by fitting the data to the simplified binding equation as above.

TIRF microscopy—In nucleation assays, assembly of 2 μ M actin was initiated by the addition of KMEH with or without Fhod. After five minutes, actin was removed from the reaction and stabilized by diluting 10-fold in 1x KMEH supplemented with Alexa Fluor 488-phalloidin. Actin was incubated with phalloidin for ten minutes, diluted 20-fold in 1x KMEH supplemented with 100 mM DTT, spotted on a poly-L-lysine-coated coverslip, and imaged. All steps were performed as delicately as possible with a cut pipet tip to minimize shearing.

For elongation experiments, biotinylated coverslips were prepared as follows. Coverslips were rinsed three times in MilliQ water, placed in 2% Hellmanex (Hellma Analytics) at 60-65 °C for 2 hours, then rinsed another five times in MilliQ water. Once dry, the coverslips were silanized with GOPTS for 1 hour in a hybridization oven. Unreacted GOPTS was removed by rinsing three times with acetone. Coverslips were then PEGylated with a mixture of methoxy-PEG-NHS and biotin-PEG-NHS as described (44).

Flow chambers of about 15 μ L were assembled on the slide using strips of double-sided tape. Flow chambers were prepared with the following steps: 1) block with 25 μ L 1% Pluronic F-127 (Sigma), 50 μ g/mL casein, in PBS, for 2 minutes; 2) 25 μ L 1x KMEH; 3) 25 μ L 40 nM streptavidin in 1x KMEH; 4) 25 μ L 1x TIRF buffer [1x KMEH, 0.5% methylcellulose (400 cP, Sigma), 50 mM DTT, 0.2 mM ATP, 20 mM glucose]; 5) 50 μ L Mg-actin and additional proteins to be assayed, in 1x TIRF buffer supplemented with 5 nM F-actin seeds (1% biotinylated, stabilized with Alexa Fluor 647-phalloidin), 250 μ g/mL glucose oxidase, 50 μ g/mL catalase, and 50 μ g/mL casein. Fhod was incubated with seeds for at least 30 seconds prior to addition of Mg-actin; in experiments with both Fhod and capping protein, Fhod was incubated with seeds for 15 seconds prior to addition of capping protein, and Mg-actin was added after an additional 30 seconds.

To determine the characteristic run length of Fhod on barbed ends in the presence of capping protein, 1 - cumulative frequency was treated as the fraction of filaments that were still elongating at a particular length. The data were fit to the exponential equation, $1 - cf = e^{-l/\lambda} * a + b$, where cf is the cumulative frequency, l is the filament length, and λ is the characteristic run length.

Reannealing assays were conducted essentially as described (47) using Alexa Fluor 488- or rhodamine-labeled phalloidin-actin, sheared by passing three times through a 27-gauge needle. Final concentrations were 250 nM F-actin and 10 nM Fhod. Samples were diluted 50-fold, spotted on poly-L-lysine-coated coverslips, and imaged.

In all experiments, actin filaments were visualized on a DMI6000 TIRF microscope (Leica) with an HCX PL APO objective (100x magnification, N.A.=1.47), and an Andor DU-897 camera, using the Leica Application Suite Advanced Fluorescence software. Experiments were conducted at room temperature. Images were obtained at 10 second intervals for 10 minutes. Images were processed by applying rolling ball background subtraction and a Gaussian filter. Filament lengths were quantified using the JFilament plugin for Fiji (48).

Cosedimentation—For high speed cosedimentation, 250 nM Fhod was incubated with varying concentrations of phalloidin-stabilized F-actin for 30 minutes at room temperature. Samples were centrifuged at 90,000 rpm for 25 minutes in a TLA-100 rotor. Pellets were concentrated by resuspending in one fourth the original volume. Supernatants and pellets were analyzed with SDS-PAGE, and gels were stained with SyproRed. The amount of Fhod in each fraction was quantified using QuantityOne software, dividing the intensities of pellet bands by four to correct for the four-fold concentration of pellets with resuspension. The fraction of Fhod bound to F-actin was calculated by adjusting for the amount of Fhod that pellets in the absence of F-actin with the following equation: $\theta = (p - p_0) / (1 - p_0)$, where θ is the fraction of Fhod bound to F-actin, p is the fraction of Fhod in the pellet, and p_0 is the fraction of Fhod in the pellet in the absence of F-actin. The affinity of Fhod for F-actin was determined by fitting the data to the

Fhod nucleates actin

binding equation, $\theta = [\text{F-actin}] / ([\text{F-actin}] + K_d) * a + b$.

For low speed cosedimentation, Fhod was incubated with phalloidin-stabilized actin filaments (final concentration of 5 μM) for 1 hour

at room temperature, then centrifuged at 12,000 x g for 15 minutes. The amount of actin in the supernatants and pellets was quantified by Coomassie-staining SDS-PAGE gels.

Acknowledgments: We thank members of the Quinlan and Reisler labs for discussions and feedback.

Conflict of interest: The authors declare that they have no conflicts of interest with the contents of this article.

Author contributions: All authors contributed to design of the experiments. A.A.P., Z.A.O.D., and A.P.v.L. performed experiments. A.A.P. and M.E.Q. wrote the manuscript with revisions from Z.A.O.D. and A.P.v.L.

REFERENCES

1. Goode, B. L., and Eck, M. J. (2007) Mechanism and Function of Formins in the Control of Actin Assembly. *Annu. Rev. Biochem.* **76**, 593–627
2. Gasteier, J. E., Madrid, R., Krautkrämer, E., Schröder, S., Muranyi, W., Benichou, S., and Fackler, O. T. (2003) Activation of the Rac-binding partner FHOD1 induces actin stress fibers via a ROCK-dependent mechanism. *J. Biol. Chem.* **278**, 38902–38912
3. Schulze, N., Graessl, M., Blancke Soares, A., Geyer, M., Dehmelt, L., and Nalbant, P. (2014) FHOD1 regulates stress fiber organization by controlling the dynamics of transverse arcs and dorsal fibers. *J. Cell Sci.* **127**, 1379–1393
4. Takeya, R., Taniguchi, K., Narumiya, S., and Sumimoto, H. (2008) The mammalian formin FHOD1 is activated through phosphorylation by ROCK and mediates thrombin-induced stress fibre formation in endothelial cells. *EMBO J.* **27**, 618–628
5. Jurmeister, S., Baumann, M., Balwiercz, A., Keklikoglou, I., Ward, A., Uhlmann, S., Zhang, J. D., Wiemann, S., and Sahin, Ö. (2012) MicroRNA-200c represses migration and invasion of breast cancer cells by targeting actin-regulatory proteins FHOD1 and PPM1F. *Mol. Cell. Biol.* **32**, 633–651
6. Iskratsch, T., Yu, C. H., Mathur, A., Liu, S., Stévenin, V., Dwyer, J., Hone, J., Ehler, E., and Sheetz, M. (2013) FHOD1 is needed for directed forces and adhesion maturation during cell spreading and migration. *Dev. Cell.* **27**, 545–559
7. Koka, S., Neudauer, C. L., Li, X., Lewis, R. E., McCarthy, J. B., and Westendorf, J. J. (2003) The formin-homology-domain-containing protein FHOD1 enhances cell migration. *J. Cell Sci.* **116**, 1745–1755
8. Gardberg, M., Kaipio, K., Lehtinen, L., Mikkonen, P., Heuser, V. D., Talvinen, K., Iljin, K., Kampf, C., Uhlen, M., Grénman, R., Koivisto, M., and Carpen, O. (2013) FHOD1, a Formin Upregulated in Epithelial-Mesenchymal Transition, Participates in Cancer Cell Migration and Invasion. *PLoS One*. 10.1371/journal.pone.0074923
9. Paul, N. R., Allen, J. L., Chapman, A., Morlan-Mairal, M., Zindy, E., Jacquemet, G., Fernandez del Ama, L., Ferizovic, N., Green, D. M., Howe, J. D., Ehler, E., Hurlstone, A., and Caswell, P. T. (2015) $\alpha 5 \beta 1$ integrin recycling promotes Arp2/3-independent cancer cell invasion via the formin FHOD3. *J. Cell Biol.* **210**, 1013–1031
10. Monzo, P., Chong, Y. K., Guetta-Terrier, C., Krishnasamy, A., Sathe, S. R., Yim, E. K. F., Ng, W. H., Ang, B. T., Tang, C., Ladoux, B., Gauthier, N. C., and Sheetz, M. P. (2016) Mechanical confinement triggers glioma linear migration dependent on formin FHOD3. *Mol. Biol. Cell.* **27**, 1246–1261
11. Krainer, E. C., Ouderkirk, J. L., Miller, E. W., Miller, M. R., Mersich, A. T., and Blystone, S. D. (2013) The multiplicity of human formins: Expression patterns in cells and tissues. *Cytoskelet.* **70**, 424–438
12. Iskratsch, T., Lange, S., Dwyer, J., Kho, A. L., dos Remedios, C., and Ehler, E. (2010) Formin follows function: a muscle-specific isoform of FHOD3 is regulated by CK2 phosphorylation and promotes myofibril maintenance. *J. Cell Biol.* **191**, 1159–1172
13. Taniguchi, K., Takeya, R., Suetsugu, S., Kan-o, M., Narusawa, M., Shiose, A., Tominaga, R., and Sumimoto, H. (2009) Mammalian formin Fhod3 regulates actin assembly and sarcomere organization in striated muscles. *J. Biol. Chem.* **284**, 29873–29881
14. Fujimoto, N., Kan-o, M., Ushijima, T., Kage, Y., and Tominaga, R. (2016) Transgenic Expression of the Formin Protein Fhod3 Selectively in the Embryonic Heart : Role of Actin-Binding Activity of Fhod3 and Its Sarcomeric Localization during Myofibrillogenesis. *PLoS One*. 10.1371/journal.pone.0148472
15. Kan-o, M., Takeya, R., Taniguchi, K., Tanoue, Y., Tominaga, R., and Sumimoto, H. (2012) Expression and subcellular localization of mammalian formin Fhod3 in the embryonic and adult heart. *PLoS One*. 10.1371/journal.pone.0034765

16. Wooten, E. C., Hebl, V. B., Wolf, M. J., Greytak, S. R., Orr, N. M., Draper, I., Calvino, J. E., Kapur, N. K., Maron, M. S., Kullo, I. J., Ommen, S. R., Bos, J. M., Ackerman, M. J., and Huggins, G. S. (2013) Formin homology 2 domain containing 3 variants associated with hypertrophic cardiomyopathy. *Circ. Cardiovasc. Genet.* **6**, 10–18
17. Dwyer, J., Pluess, M., Iskratsch, T., dos Remedios, C. G., and Ehler, E. (2014) The formin FHOD1 in cardiomyocytes. *Anat. Rec.* **297**, 1560–1570
18. Arimura, T., Takeya, R., Ishikawa, T., Yamano, T., Matsuo, A., Tatsumi, T., Nomura, T., Sumimoto, H., and Kimura, A. (2013) Dilated Cardiomyopathy-Associated FHOD3 Variant Impairs the Ability to Induce Activation of Transcription Factor Serum Response Factor. *Circ. J.* **77**, 2990–2996
19. Esslinger, U., Garnier, S., Korniat, A., Proust, C., Kararigas, G., Müller-Nurasyid, M., Empana, J.-P., Morley, M. P., Perret, C., Stark, K., Bick, A. G., Prasad, S. K., Kriebel, J., Li, J., Tired, L., Strauch, K., O'Regan, D. P., Marguiles, K. B., Seidman, J. G., Boutouyrie, P., Lacolley, P., Jouven, X., Hengstenberg, C., Komajda, M., Hakonarson, H., Isnard, R., Arbustini, E., Grallert, H., Cook, S. A., Seidman, C. E., Regitz-Zagrosek, V., Cappola, T. P., Charron, P., Cambien, F., and Villard, E. (2017) Exome-wide association study reveals novel susceptibility genes to sporadic dilated cardiomyopathy. *PLoS One*. 10.1371/journal.pone.0172995
20. Schönichen, A., Mannherz, H. G., Behrmann, E., Mazur, A. J., Kühn, S., Silván, U., Schoenenberger, C.-A., Fackler, O. T., Raunser, S., Dehmelt, L., and Geyer, M. (2013) FHOD1 is a combined actin filament capping and bundling factor that selectively associates with actin arcs and stress fibers. *J. Cell Sci.* **126**, 1891–1901
21. Lammel, U., Bechtold, M., Risse, B., Berh, D., Fleige, A., Bunse, I., Jiang, X., Klämbt, C., and Bogdan, S. (2014) The Drosophila FHOD1-like formin Knittrig acts through Rok to promote stress fiber formation and directed macrophage migration during the cellular immune response. *Development*. **141**, 1366–1380
22. Shwartz, A., Dhanyasi, N., Schejter, E. D., and Shilo, B.-Z. (2016) The Drosophila formin Fhos is a primary mediator of sarcomeric thin-filament array assembly. *Elife*. 10.7554/eLife.16540.001
23. Kucherenko, M. M., Marrone, A. K., Rishko, V. M., Magliarelli, H. D. F., and Shcherbata, H. R. (2011) Stress and muscular dystrophy: A genetic screen for Dystroglycan and Dystrophin interactors in Drosophila identifies cellular stress response components. *Dev. Biol.* **352**, 228–242
24. Xu, Y., Moseley, J. B., Sagot, I., Poy, F., Pellman, D., Goode, B. L., and Eck, M. J. (2004) Crystal structures of a formin homology-2 domain reveal a tethered dimer architecture. *Cell*. **116**, 711–723
25. Bombardier, J. P., Eskin, J. A., Jaiswal, R., Corrêa, I. R., Xu, M.-Q., Goode, B. L., and Gelles, J. (2015) Single-molecule visualization of a formin-capping protein “decision complex” at the actin filament barbed end. *Nat. Commun.* 10.1038/ncomms9707
26. Shekhar, S., Kerleau, M., Kühn, S., Pernier, J., Romet-Lemonne, G., Jégou, A., and Carlier, M.-F. (2015) Formin and capping protein together embrace the actin filament in a ménage à trois. *Nat. Commun.* 10.1038/ncomms9730
27. Barko, S., Bugyi, B., Carlier, M. F., Gombos, R., Matusek, T., Mihályand, J., and Nyitrai, M. (2010) Characterization of the biochemical properties and biological function of the formin homology domains of Drosophila DAAM. *J. Biol. Chem.* **285**, 13154–13169
28. Harris, E. S., Li, F., and Higgs, H. N. (2004) The Mouse Formin, FRLa, Slows Actin Filament Barbed End Elongation, Competes with Capping Protein, Accelerates Polymerization from Monomers, and Severs Filaments. *J. Biol. Chem.* **279**, 20076–20087
29. Kovar, D. R., Kuhn, J. R., Tichy, A. L., and Pollard, T. D. (2003) The fission yeast cytokinesis formin Cdc12p is a barbed end actin filament capping protein gated by profilin. *J. Cell Biol.* **161**, 875–887
30. Paul, A., and Pollard, T. (2008) The Role of the FH1 Domain and Profilin in Formin-Mediated Actin-Filament Elongation and Nucleation. *Curr. Biol.* **18**, 9–19
31. Courtemanche, N., and Pollard, T. D. (2012) Determinants of formin homology 1 (FH1) domain function in actin filament elongation by formins. *J. Biol. Chem.* **287**, 7812–7820

32. Kovar, D. R., Harris, E. S., Mahaffy, R., Higgs, H. N., and Pollard, T. D. (2006) Control of the assembly of ATP- and ADP-actin by formins and profilin. *Cell*. **124**, 423–435
33. Vizcarra, C. L., Bor, B., and Quinlan, M. E. (2014) The Role of Formin Tails in Actin Nucleation, Processive Elongation, and Filament Bundling. *J. Biol. Chem.* **289**, 30602–30613
34. Scott, B. J., Neidt, E. M., and Kovar, D. R. (2011) The functionally distinct fission yeast formins have specific actin-assembly properties. *Mol. Biol. Cell*. **22**, 3826–3839
35. Michelot, A., Guérin, C., Huang, S., Ingouff, M., Richard, S., Rodiuc, N., Staiger, C. J., and Blanchoin, L. (2005) The Formin Homology 1 Domain Modulates the Actin Nucleation and Bundling Activity of Arabidopsis FORMIN1. *Plant Cell*. **17**, 2296–2313
36. Li, F., and Higgs, H. N. (2003) The Mouse Formin mDia1 Is a Potent Actin Nucleation Factor Regulated by Autoinhibition. *Curr. Biol.* **13**, 1335–1340
37. Henty-Ridilla, J. L., Rankova, A., Eskin, J. A., Kenny, K., and Goode, B. L. (2016) Accelerated actin filament polymerization from microtubule plus ends. *Science*. **352**, 1004–1009
38. Liu, H., and Naismith, J. H. (2008) An efficient one-step site-directed deletion, insertion, single and multiple-site plasmid mutagenesis protocol. *BMC Biotechnol.* 10.1186/1472-6750-8-91
39. Zuchero, J. B. (2007) In vitro actin assembly assays and purification from Acanthamoeba. *Methods Mol. Biol.* **370**, 213–226
40. Grintsevich, E. E., Yesilyurt, H. G., Rich, S. K., Hung, R., and Terman, J. R. (2016) F-actin dismantling through a redox-driven synergy between Mical and cofilin. **18**, 876–885
41. Roth-Johnson, E. A., Vizcarra, C. L., Bois, J. S., and Quinlan, M. E. (2014) Interaction between microtubules and the Drosophila formin cappuccino and its effect on actin assembly. *J. Biol. Chem.* **289**, 4395–4404
42. Lu, J., and Pollard, T. D. (2001) Profilin Binding to Poly-L-Proline and Actin Monomers along with Ability to Catalyze Actin Nucleotide Exchange Is Required for Viability of Fission Yeast. *Mol. Biol. Cell*. **12**, 1161–1175
43. Palmgren, S., Ojala, P. J., Wear, M. A., Cooper, J. A., and Lappalainen, P. (2001) Interactions with PIP2, ADP-actin monomers, and capping protein regulate the activity and localization of yeast twinfilin. *J. Cell Biol.* **155**, 251–260
44. Bor, B., Vizcarra, C. L., Phillips, M. L., and Quinlan, M. E. (2012) Autoinhibition of the formin Cappuccino in the absence of canonical autoinhibitory domains. *Mol. Biol. Cell*. **23**, 3801–3813
45. Pollard, T. D. (1986) Rate constants for the reactions of ATP-and ADP-actin with the ends of actin filaments. *J. Cell Biol.* **103**, 2747–2754
46. Vinson, V. K., De La Cruz, E. M., Higgs, H. N., and Pollard, T. D. (1998) Interactions of Acanthamoeba profilin with actin and nucleotides bound to actin. *Biochemistry*. **37**, 10871–10880
47. Vizcarra, C. L., Kreutz, B., Rodal, A. A., Toms, A. V., Lu, J., Zheng, W., Quinlan, M. E., and Eck, M. J. (2011) Structure and function of the interacting domains of Spire and Fmn-family formins. *Proc. Natl. Acad. Sci. U. S. A.* **108**, 11884–11889
48. Smith, M. B., Li, H., Shen, T., Huang, X., Yusuf, E., and Vavylonis, D. (2010) Segmentation and tracking of cytoskeletal filaments using open active contours. *Cytoskeleton*. **67**, 693–705

FOOTNOTES

This work was supported by the following grants from the National Institutes of Health: NRSA F30 HL137263 (A.A.P.), UCLA Medical Scientist Training Program T32 GM008042 (A.A.P.), and R01 GM096133 (M.E.Q.). The content is solely the responsibility of the authors and does not necessarily represent the official views of the National Institutes of Health.

The abbreviations used are: FHOD, formin homology domain-containing protein; TIRF, total internal reflection fluorescence; FH, formin homology domain; IPTG, isopropyl β -D-thiogalactoside; DTT, dithiothreitol; PMSF, phenylmethanesulfonyl fluoride; EGTA, ethylene glycol tetraacetic acid ; GOPTS, (3-glycidyloxypropyl)trimethoxysilane

FIGURE LEGENDS

FIGURE 1. The *Drosophila* formin Fhod accelerates actin assembly. *A*, domain structure of Fhod isoform A. Fhod includes formin homology domains for actin assembly and the Diaphanous inhibitory domain (DID) and Diaphanous autoregulatory domain (DAD) for autoinhibition and regulation. The Fhod construct used in this work spans residues 638-1393 and includes the FH1 domain, FH2 domain, and tail. *B*, assembly of 2 μ M *Acanthamoeba castellanii* actin (10% pyrene-labeled) in the absence (black) or presence (blue) of 1-8 nM Fhod. Fhod accelerates actin assembly in a dose-dependent manner. *C*, quantification of barbed end concentrations at the time to half-polymerization from *B*. Data represent the mean \pm standard deviation from two independent experiments. *D*, assembly of 2 μ M amoeba actin (10% pyrene-labeled) in the presence of 16 nM wild-type (blue) or mutant (I966A, red; K1112A, green) Fhod. Actin assembly by Fhod is reduced moderately by the K1112A mutation and severely by the I966A mutation. *E*, assembly of 2 μ M amoeba actin (5% pyrene-labeled) in the presence of 4 μ M *S. pombe* profilin and the indicated concentrations of Fhod. Fhod accelerates actin assembly in the presence of profilin.

FIGURE 2. Fhod promotes actin nucleation, but not elongation. *A*, 2 μ M actin was polymerized in the absence (left) or presence (right) of 8 nM Fhod for 5 minutes, then stabilized with Alexa Fluor 488-phalloidin and imaged by TIRF microscopy. Scale bar is 10 μ m. *B*, quantification of *A*. Fhod increases the number of actin filaments per field of view. Data are from three independent experiments for each condition. Lines represent the mean. *C*, actin elongation from preformed seeds. Final conditions were 0.25 μ M F-actin seeds (\sim 0.4 nM barbed ends), 0.5 μ M G-actin (10% pyrene-labeled), in the absence (black) or presence (blue) of 1.5-48 nM Fhod. Fhod slows barbed end elongation in a dose-dependent manner. *D*, actin elongation from preformed seeds, as in *C*, with 1.5 μ M *S. pombe* profilin. Fhod does not slow elongation in the presence of profilin. *E*, quantification of elongation rates from *C* and *D*. Elongation rates were measured as the initial slope over the first 90 seconds, relative to the slope of actin alone. Fhod substantially slows elongation only in the absence of profilin. The data and reported K_d are the mean \pm standard deviation from 3 independent experiments. The binding curve shows the best fit to the average values. *F*, direct observation of barbed end elongation by TIRF microscopy with 5 nM F-actin seeds (1% biotinylated, labeled with Alexa Fluor 647-phalloidin), 1 μ M G-actin (10% Alexa Fluor 594-labeled) and 5 μ M *S. pombe* profilin, \pm 4 nM Fhod. Images were taken 8 minutes after the start of polymerization. Scale bar is 10 μ m. *G*, quantification of elongation from *F*. Ten representative traces from each condition are plotted. Elongation rates are average \pm standard deviation from 3 flow chambers for each condition.

FIGURE 3. Fhod binds barbed ends. *A*, actin filaments were depolymerized by dilution to 0.1 μ M (70% pyrene-labeled) with varying concentrations of Fhod. Data were normalized against the initial pyrene fluorescence. *B*, quantification of depolymerization rates from *A*, represented by the initial slope over the first 90 seconds. Fhod binds barbed ends and slows depolymerization. The data and reported K_d are the mean \pm standard deviation from six independent experiments. The binding curve shows the best fit to the average values. *C*, Actin filaments, stabilized with Alexa Fluor 488- (green) or rhodamine- (magenta)

Fhod nucleates actin

phalloidin, were sheared and allowed to reanneal for 30 minutes. Final concentrations were 0.25 μ M F-actin \pm 10 nM Fhod. Fhod inhibits reannealing of the sheared filaments. Scale bar is 10 μ m.

FIGURE 4. Fhod antagonizes capping protein. *A*, actin elongation from preformed seeds with a range of Fhod concentrations added before capping protein. Final conditions were 0.25 μ M F-actin seeds (\sim 0.4 nM barbed ends), 0.5 μ M G-actin (10% pyrene-labeled), 1.5 μ M *S. pombe* profilin, \pm 6 nM mouse capping protein and 1.5-48 nM Fhod. *B*, quantification of elongation rates from *A*, measured as the initial slope over the first 90 seconds relative to the slope of actin alone. Fhod antagonizes capping protein, allowing elongation. Data with Fhod and capping protein were fit to a competition binding model to determine the affinity of Fhod to barbed ends. The data and reported K_d are mean \pm standard deviation from four independent experiments. The binding curve shows the best fit to the average values. *C*, observation of actin elongation (white) from preformed seeds (green) with Fhod added before capping protein. Final conditions were 5 nM F-actin seeds (1% biotinylated, labeled with Alexa Fluor 647-phalloidin), 1 μ M G-actin (10% Alexa Fluor 594-labeled), 5 μ M *S. pombe* profilin, \pm 2 nM Fhod and 6 nM capping protein. Images were taken five minutes after the start of polymerization. Scale bar is 10 μ m. *D*, quantification of filament lengths from *C*. Data represent the amount of elongation from preformed seeds ($n > 150$ for each condition). At least 5 fields of view from 1 (actin alone) or 2 (all other conditions) flow chambers were analyzed for each condition. In conditions with capping protein, no box is visible because over 75% of seeds did not elongate. *E*, exponential fit of filament lengths in the presence of both Fhod and capping protein from *D*, excluding seeds that did not elongate ($n=69$ filaments from 2 flow chambers).

FIGURE 5. Fhod binds the sides of actin filaments and forms actin bundles. *A*, high speed cosedimentation assay with 250 nM Fhod and varying concentrations of phalloidin-actin. The fraction of Fhod bound to F-actin was quantified by measuring the amount of Fhod in the pellet and correcting for the amount of Fhod that pellets in the absence of F-actin. The data and reported K_d are mean \pm standard deviation from three independent experiments. The binding curve shows the best fit to the average values. *B*, low speed cosedimentation assay with 5 μ M phalloidin-actin and varying concentrations of Fhod. Data are mean \pm standard deviation from two independent experiments. *C*, representative images of Fhod-induced actin bundles visualized by TIRF microscopy. Final conditions were 5 nM F-actin seeds (1% biotinylated, labeled with Alexa Fluor 647-phalloidin), 1 μ M G-actin (10% Alexa Fluor 594-labeled), 5 μ M *S. pombe* profilin, 4 nM Fhod. Bundles elongate at both ends, indicating mixed or antiparallel polarity. Scale bar is 10 μ m.

Figure 1

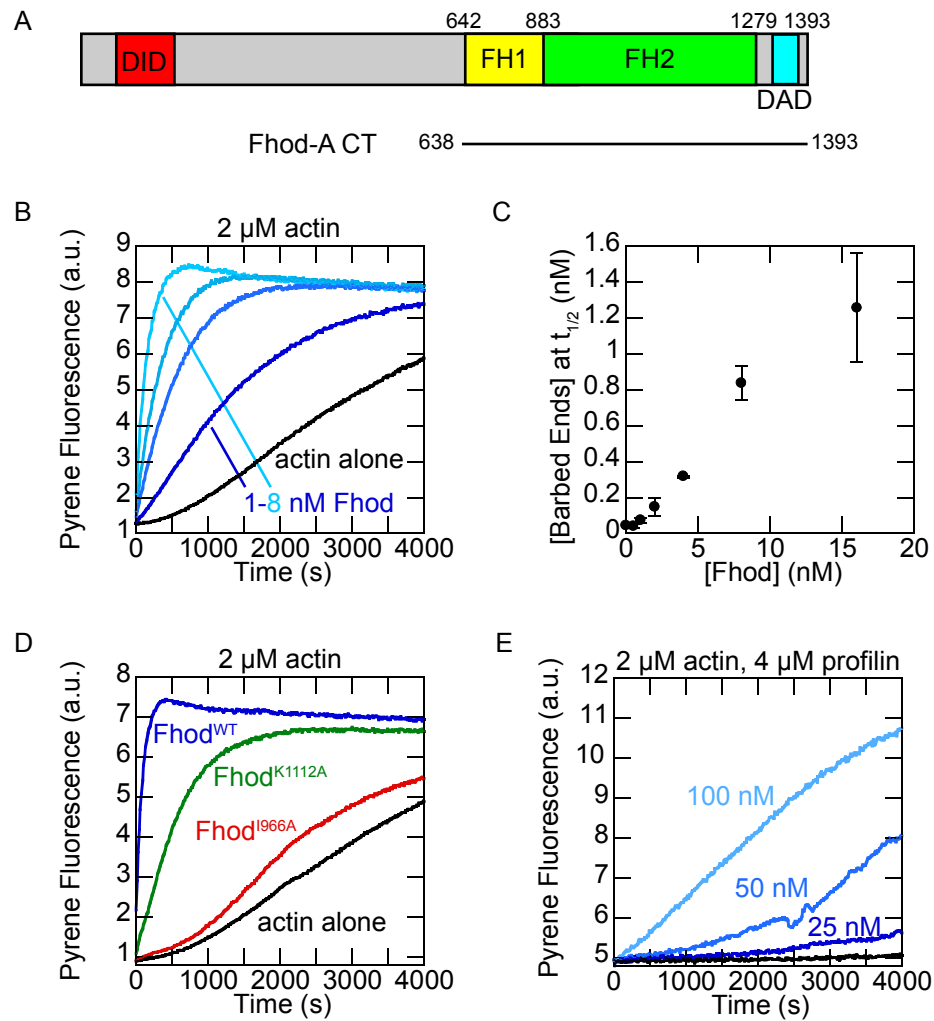


Figure 2

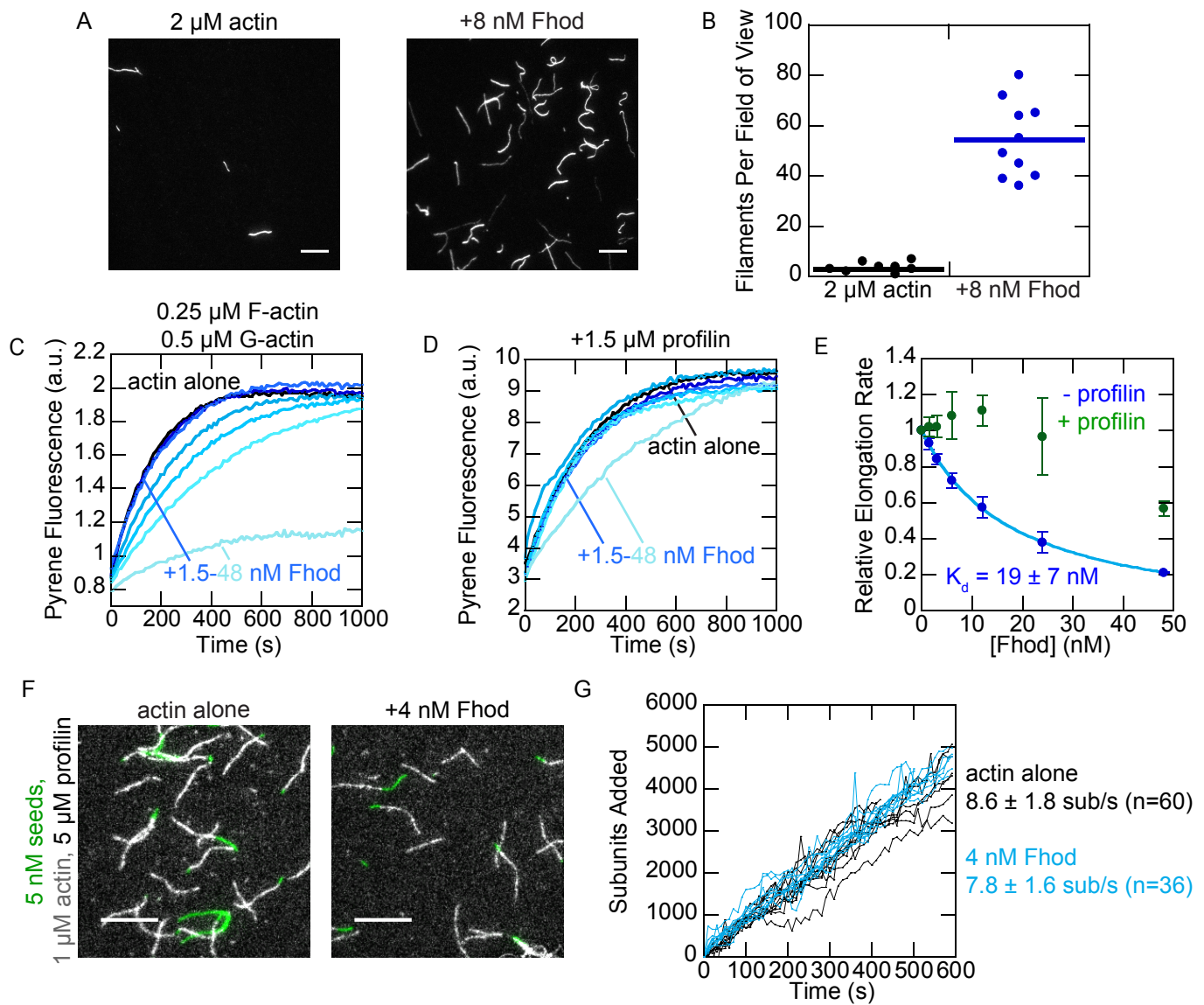


Figure 3

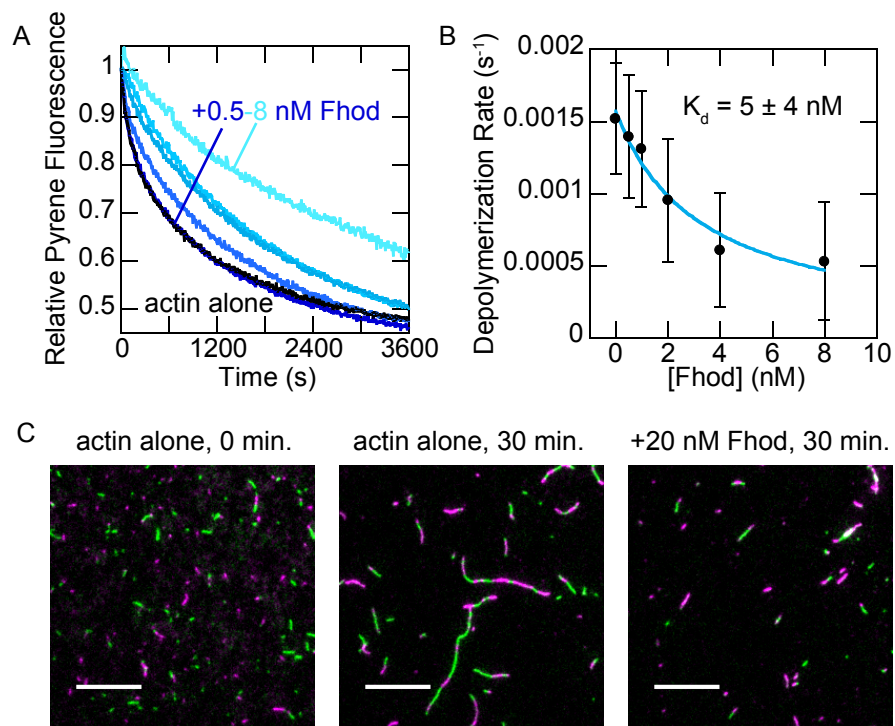


Figure 4

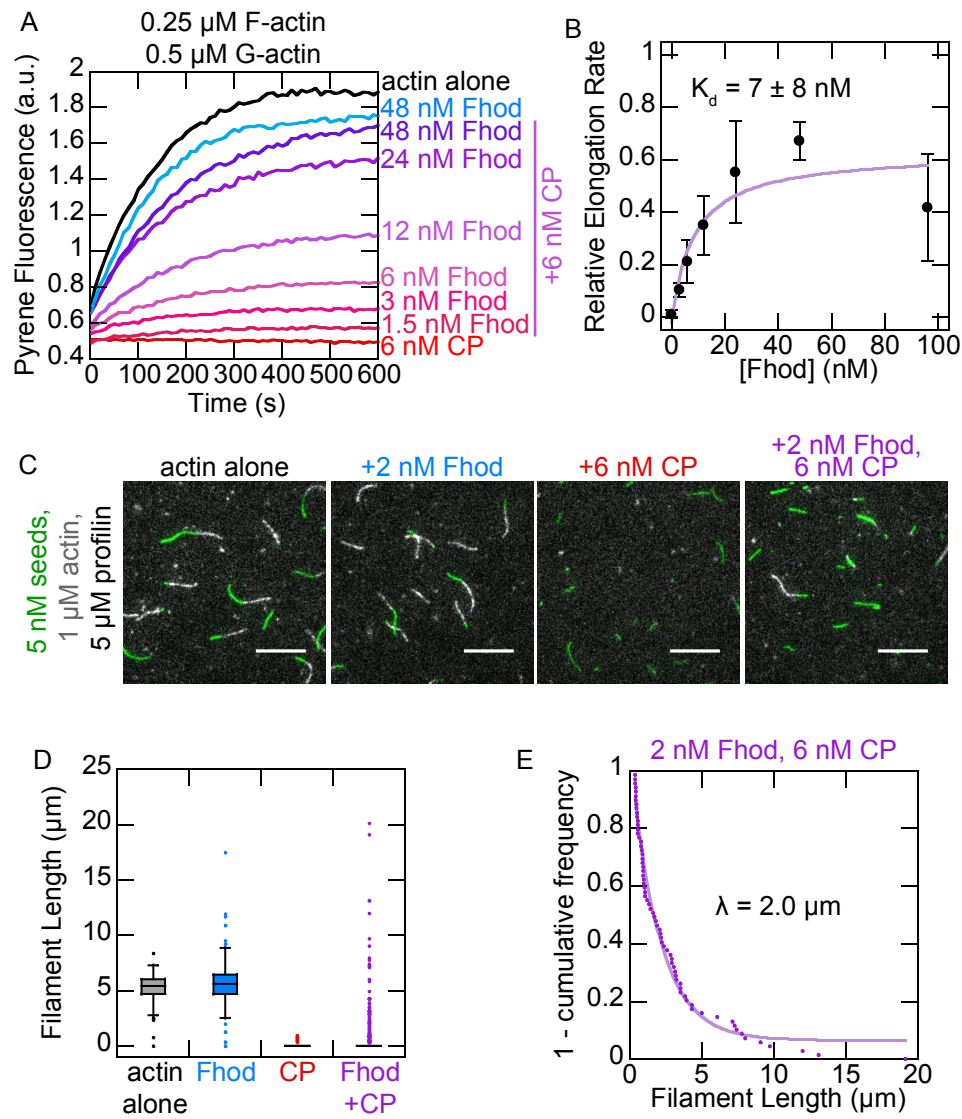


Figure 5

